

Improving Electrochemical Stability and Low-Temperature Performance with Water/Acetonitrile Hybrid Electrolytes

Jiawei Chen, Jenel Vatamanu, Lidan Xing,* Oleg Borodin, Huiyang Chen, Xiongcong Guan, Xiang Liu, Kang Xu,* and Weishan Li

Although the “water-in-salt” electrolyte has significantly expanded the electrochemical stability window of aqueous electrolytes from 1.23 to 3 V, its inevitable hydrogen evolution under 1.9 V versus Li⁺/Li prevents the practical use of many energy-dense anodes. Meanwhile, its liquidus temperature at 17 °C restricts its application below ambient temperatures. An advanced hybrid electrolyte is proposed in this work by introducing acetonitrile (AN) as co-solvent, which minimizes the presence of interfacial water at the negatively charged electrode surface, and generates a thin and uniform interphase consisting of an organic outer layer based on nitrile (C≡N) and sulfamide (R-S-N-S) species and an inner layer rich in LiF. Such an interphase significantly suppresses water reduction and expands the electrochemical stability window to an unprecedented width of 4.5 V. Thanks to the low freezing point (−48 °C) and low viscosity of AN, the hybrid electrolyte is highly conductive in a wide temperature range, and enables a LiMn₂O₄/Li₄Ti₅O₁₂ full cell at both ambient and sub-ambient temperatures with excellent cycling stability and rate capability. Meanwhile, such a hybrid electrolyte also inherits the nonflammable nature of aqueous electrolyte. The well-balanced merits of the developed electrolyte make it suitable for high energy density aqueous batteries.

headlines,^[3–5] for which the highly flammable nonaqueous electrolytes used in LIBs are mainly responsible. It is under this context that aqueous LIBs (ALIBs) are revisited as a fundamental solution to safety, despite their low energy densities due to the narrow electrochemical stability window of water.^[2,6–10] Recently, a new class of high-voltage aqueous electrolyte was discovered by dissolving 21 molality (mol) lithium bis(trifluoromethane sulfonyl) imide (LiTFSI) in 1 kg of water. Such a “water-in-salt” electrolyte (WiSE) expands the electrochemical stability window from 1.23 to 3.0 V, which supports a 2.5 V chemistry using LiMn₂O₄ (LMO) cathode and Mo₆S₈ anode to stably deliver ≈100 Wh kg^{−1} for thousand cycles. The significantly improved electrochemical stability therein mainly comes from the depletion of free water molecules and the formation of an anion-derived solid-electrolyte interphase (SEI) on the anode surface.^[9] However, because of the intrinsic


repulsion of anions and adsorption of the Li⁺-4(H₂O) solvates by the negatively polarized anode surface,^[4] the formation of such an anion-derived SEI has been impossible below 1.9 V versus Li⁺/Li.^[9] This “cathodic challenge” has essentially excluded many desired energy-dense anodes that operate at low potentials such as Li-metal, graphite, or silicon. Even Li₄Ti₅O₁₂ (LTO) that operates at mild potential (≈1.70 V Li⁺/Li in WiSE) suffers from irreversibility, because it sits right on the edge of the cathodic limit in WiSE. Efforts aiming to resolve the “cathodic challenge” with additional lithium salts such as lithium trifluoromethane sulfonate (LiOTf)^[11] or lithium bis(pentafluoroethane sulfonyl) imide (LiBETI)^[10] achieved limited success, because solubility limits of the salts impose restrictions on how high their concentration can go, while the effectiveness of added anions still faces intrinsic resistance from anode surface against their accumulation at inner-Helmholtz layer, not to mention that these additional salts further worsen the already problematic viscosity and ionic conductivity of WiSE. Introducing a non-aqueous solvent, dimethyl carbonate (DMC),^[12] into WiSE expands the electrochemical window of the hybrid electrolyte to 4.1 V, because the neutral solvent is less sensitive to anode repulsion and hence participates in interphasial chemistry more easily than anions. The additional protection from an SEI consisting of both anion- and solvent-derived products enables LTO operation

1. Introduction

Lithium-ion batteries (LIBs) keep finding new applications in our life,^[1,2] but accordingly their safety also raises public concerns as increasingly frequent battery fires are reported in

J. Chen, Prof. L. Xing, H. Chen, X. Guan, Prof. X. Liu, Prof. W. Li
National and Local Joint Engineering Research Center of MPES
in High Energy and Safety LIBs
Engineering Research Center of MTEES (Ministry of Education)
Research Center of BMET (Guangdong Province)
Key Laboratory of ETESPG (GHEI)
Innovative Platform for ITBMD (Guangzhou Municipality)
School of Chemistry
South China Normal University
Guangzhou 510006, China
E-mail: xingld@scnu.edu.cn

Dr. J. Vatamanu, Dr. O. Borodin, Dr. K. Xu
Battery Branch
Sensor and Electron Devices Directorate
U.S. Army Research Laboratory
Adelphi, MD 20783, USA
E-mail: conrad.k.xu.civ@mail.mil

 The ORCID identification number(s) for the author(s) of this article can be found under <https://doi.org/10.1002/aenm.201902654>.

DOI: 10.1002/aenm.201902654

in the resultant hybrid aqueous/nonaqueous electrolyte. However, the moderate viscosity^[13] and high freezing point (4.6 °C)^[14] of DMC still prevent the application of such hybrid electrolyte at low temperatures. In a similar approach, a hybrid “acetonitrile (AN)/water in salt” electrolyte (AN-WiSE) system was also reported, providing improved ionic conductivity, reduced viscosity, and expanded temperature range for the application in supercapacitors.^[15] Perhaps in order to circumvent the formation of any interphase, which would eliminate the high surface area that double-layer capacitance relies on, only 5 mol LiTFSI was used in the AN-WiSE hybrid. In this work, we increase the LiTFSI salt concentration in AN-WiSE to the level of super-concentration (15.3 mol), where the formation of interphase is activated. An electrochemical stability window of 4.5 V is achieved by the new interphasial chemistry and the exclusion of water molecules by both TFSI anions and AN molecules at anode surface. The super-concentrated hybrid electrolyte also benefits from the advantages of AN including high dielectric constant (35.9), low freezing point (−48 °C), high oxidation stability (>5 V vs Li⁺/Li), and high miscibility with

water.^[13,16–18] These combined merits enable the ALIB based on LMO/LTO chemistry with high capacity at both room and low temperatures.

2. Results and Discussion

2.1. Structure and Physicochemical Property

Table S1 (Supporting Information) summarizes the compositions and acronyms of all hybrid electrolytes investigated in this work, with both WiSE and “bisolvent-in-salt” (BSiS)-D_{0.28} used as references. The BSiS-A electrolyte structure was investigated via Raman spectroscopy and molecular dynamics (MD) simulations. The Raman spectra were compared with those of WiSE and BSiS-D_{0.28} (Figure 1 and Figure S1, Supporting Information). The peak at 2252 cm^{−1} is ascribed to the C≡N stretching vibration in AN molecular (Figure 1A), which disappears in BSiS-A hybrid electrolytes and is replaced by two new peaks at 2263 and 2282 cm^{−1}. The peak of higher intensity at 2282 cm^{−1}

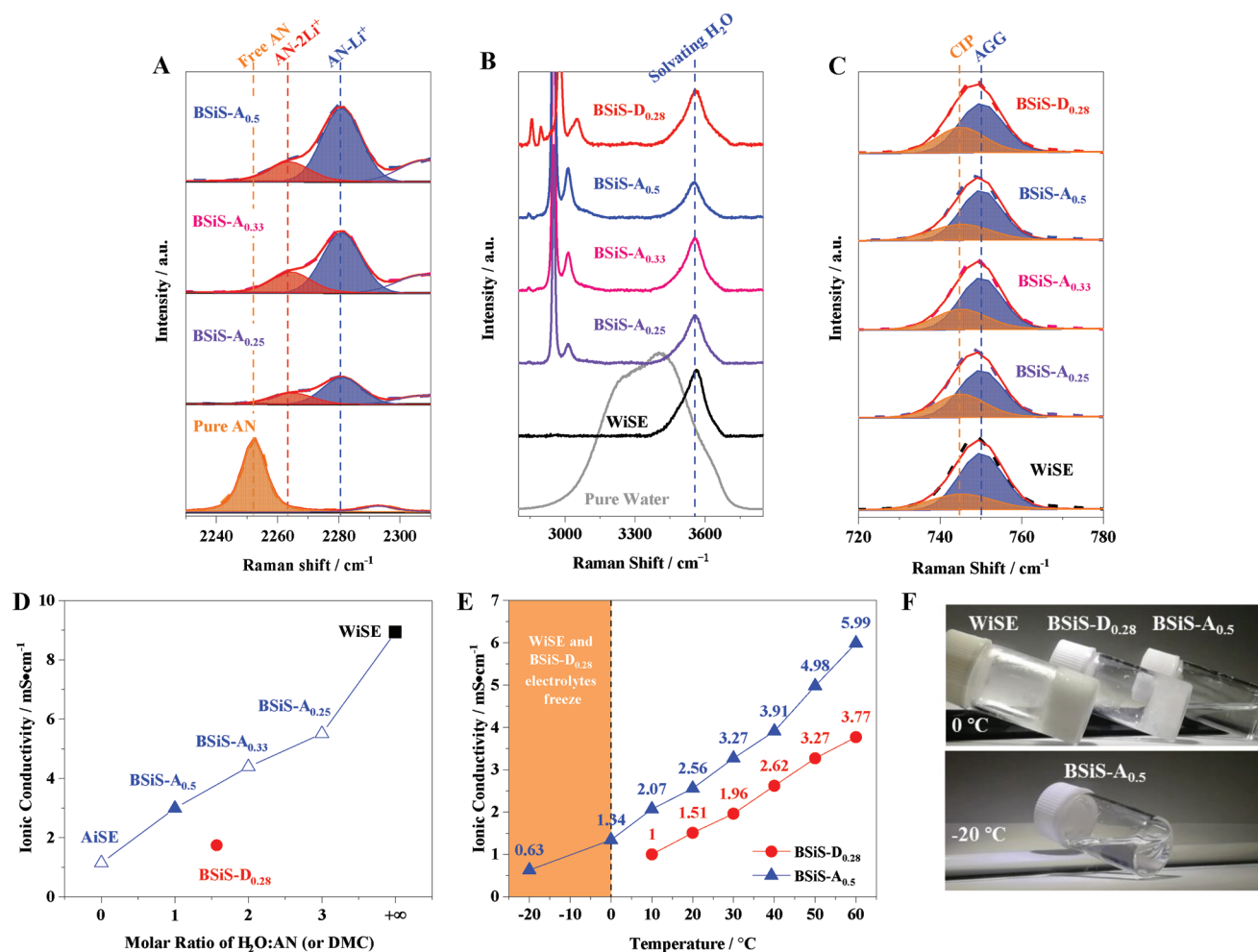


Figure 1. Raman spectra of WiSE and BSiS electrolytes compared with pure AN and water in A) 2230–2310 cm^{−1} (C≡N stretching vibration of AN), B) 2800–3850 cm^{−1} (O–H stretching vibration of H₂O), and C) 720–780 cm^{−1} (S–N–S bending vibration of TFSI[−]). D) Ionic conductivity of WiSE, BSiS, and “AN-in-salt” (AiSE, 12.8 mol LiTFSI in 1 kg AN) electrolytes at 25 °C. E) Ionic conductivity of BSiS-D_{0.28} and BSiS-A_{0.5} hybrid electrolytes in temperature range of −20 to 60 °C. F) Photographs showing the states of WiSE, BSiS-D_{0.28}, and BSiS-A_{0.5} electrolytes at 0 and −20 °C.

has been ascribed to the generation of AN-Li⁺ solvation structure,^[18] while the one of lower intensity at 2263 cm⁻¹ to the C≡N stretching vibration of AN in AN-2Li⁺ solvation structure according to our density function theory (DFT) calculations (Figure S2, Supporting Information). The complete vanishing of free AN peak at 2252 cm⁻¹ indicates that, at such super-concentration, almost all AN molecules are coordinated with Li⁺ in BSiS-A hybrid electrolytes. It should be noted that the activity of AN-2Li⁺ structure in electrochemical reduction is significantly higher than that of AN-Li⁺ and comparable with DMC-2Li⁺ (Figure S3, Supporting Information). It has been proposed that DMC-2Li⁺ reduces prior to the decomposition of water,^[12] hence AN-2Li⁺ would have the opportunity to form a protective SEI consisting of C≡N-containing products before hydrogen evolution occurs. The peak corresponding to O-H stretching vibration of H₂O molecule in BSiS-A hybrid electrolytes is similar to that of WiSE and BSiS-D_{0.28},^[10,19] indicating that almost all H₂O molecules are also coordinated with Li⁺. More detailed structural information of H₂O molecule in Li⁺-solvation sheath was further provided by ¹⁷O NMR (Figure S4, Supporting Information), where the downshift of ¹⁷O signal in LiTFSI relative to water was ascribed to the deshielding of the lone pair electrons on water by Li⁺.^[9] It can be thus inferred that the introduction of AN does not weaken the interaction of H₂O with Li⁺. Indeed, the probability of Li⁺ solvated by more than one H₂O molecule, in BSiS-A_{0.5}, Li⁺-4(H₂O) in particular, is significantly higher than that in BSiS-D_{0.28} based on MD simulation (Figure S5, Supporting Information), implying that the addition of AN co-solvent promotes the interaction of H₂O molecules and Li⁺, which would further decrease the reaction activity of water. The relative binding energies of Li⁺ to AN, DMC, H₂O, and TFSI⁻ decrease in the following order: Li⁺-TFSI⁻ > Li⁺-H₂O > Li⁺-DMC > Li⁺-AN, as shown in Figure S6 (Supporting Information), resulting in the preferential coordination of Li⁺ to H₂O instead of AN. Compared with water, the weaker capability of AN to interact with Li⁺ makes it lose the competition of forming Li⁺ solvation sheath, hence Li⁺-4(H₂O) becomes the prevailing species. On the other hand, AN and TFSI⁻ co-exist in the same solvation sheath of Li⁺ (Figure S7A, Supporting Information). The separation of AN and H₂O in different Li⁺ solvation sheaths leads to a H₂O-rich (inorganic) phase and an AN-rich (organic) phase that interpenetrate each other in the BSiS-A_{0.5} hybrid electrolyte (Figure S7B, Supporting Information), which would be beneficial to fast Li⁺ conduction due to the high fraction of the fast-moving “solvent-separated ion pairs” Li⁺-4(H₂O) and fast exchange of AN around Li⁺.^[16] In agreement with the MD simulation, Raman reveals that TFSI⁻ mainly exists as Li⁺-TFSI⁻ contact ion pairs (CIP, 745 cm⁻¹) and coordinates to two or more Li⁺ as aggregates (AGG, 750 cm⁻¹, Figure 1C) in BSiS-A hybrid electrolytes.^[18] It has been previously established that the reduction activity of TFSI⁻ AGG structure is much higher than that of a free TFSI⁻,^[9,20] leading to a high possibility of a LiF-rich interphase that is more effective in suppressing water reduction. Therefore, the dominant TFSI⁻ AGG structure in BSiS-A electrolytes would lead to the improved interfacial stability of anode/electrolyte due to earlier onset of the TFSI⁻ reduction at higher potentials.

As a result of the increased Li⁺-water interaction, the content of un-solvated (free) H₂O molecule decreases with increase of

the TFSI⁻ AGG structure proportional to the ratio of AN in BSiS-A. Among the BSiS-A hybrid electrolytes investigated, BSiS-A_{0.5} will provide higher interfacial stability at anode than the other two compositions.

The ionic conductivity of BSiS-A_{0.5} at 25 °C (2.99 mS cm⁻¹, Figure 1D) is lower than WiSE, but still higher than BSiS-D_{0.28} and other proposed concentrated nonaqueous electrolytes.^[21,22] The ionic conductivity decreases gradually with the addition of AN, while the improvement in electrochemical stability becomes constant after AN ratio reaches 0.5, therefore, further increasing the AN content beyond BSiS-A_{0.5} hybrid electrolyte brings no additional benefits. The temperature dependences of ionic conductivity for BSiS-A_{0.5} and BSiS-D_{0.28} were compared. Within the temperature range of -20 to 60 °C, the ionic conduction in BSiS-A_{0.5} is obviously faster than BSiS-D_{0.28} (Figure 1E), especially in the sub-ambient temperature regime, which should be ascribed to the low freezing temperature (see Figure S8, Supporting Information) and low viscosity of AN. In particular, both WiSE and BSiS-D_{0.28} become solid at ≈0 °C (Figure 1F top), while BSiS-A_{0.5} remains liquid (Figure 1F bottom) and provides the conductivity of 1.34 and 0.63 mS cm⁻¹ at 0 and -20 °C (Figure 1E), respectively.

The thermal stability of BSiS-A_{0.5}, BSiS-D_{0.28}, WiSE, and NCE (nonaqueous conventional electrolyte, 1 mol LiPF₆ in 1 L mixture of ethylene carbonate:ethyl methyl carbonate:diethyl carbonate = 3:5:2 by weight) was investigated using thermogravimetry (TG) and compared in Figure S9 (Supporting Information). Both dynamic (Figure S9A, Supporting Information) and isothermal (Figure S9B, Supporting Information) TG curves show that the thermal stabilities of BSiS-A_{0.5}, BSiS-D_{0.28}, and WiSE are very close and much higher than that of NCE, which should be owing to the well coordination between Li⁺ and solvent molecules (Figure 1A,B and Figure S4, Supporting Information).^[23] In stark contrast, upon heating to 150 °C or maintaining at 100 °C for 20 min, NCE suffers an almost 65% mass loss due to the evaporation and decomposition of its components. Such massive evaporation would produce dramatic internal pressure in a closed battery that either leads to cell vent or explosion. It is worth mentioning that the differences among the TG curves of BSiS-A_{0.5}, BSiS-D_{0.28}, and WiSE are negligible due to the close boiling points of AN (81 °C),^[24] DMC (91 °C),^[14] and water (100 °C). More importantly, BSiS-A_{0.5} also inherits the nonflammability of aqueous electrolytes, as shown in Videos S1 to S3 (Supporting Information).

2.2. Electrochemical Performance

The electrochemical stability of BSiS-A_{0.5}, WiSE, and BSiS-D_{0.28} electrolytes is evaluated with linear sweep voltammetry (LSV) at the scan rate of 5 mV s⁻¹ (Figure 2A), in which the cathodic (from 3 to 0.5 V vs Li⁺/Li) and anodic (from 3 to 5.5 V vs Li⁺/Li) limits were separately measured on Al and Ti substrates. Because of the “cathodic challenge,” the SEI that is only derived from TFSI⁻ in WiSE becomes unstable to suppress the reduction of water at low potential,^[4] as evidenced by the current corresponding to severe hydrogen evolution reaction below 1.6 V versus Li⁺/Li (Figure 2A). By the standard established previously,^[12] the reduction peak at around 1.5 V versus

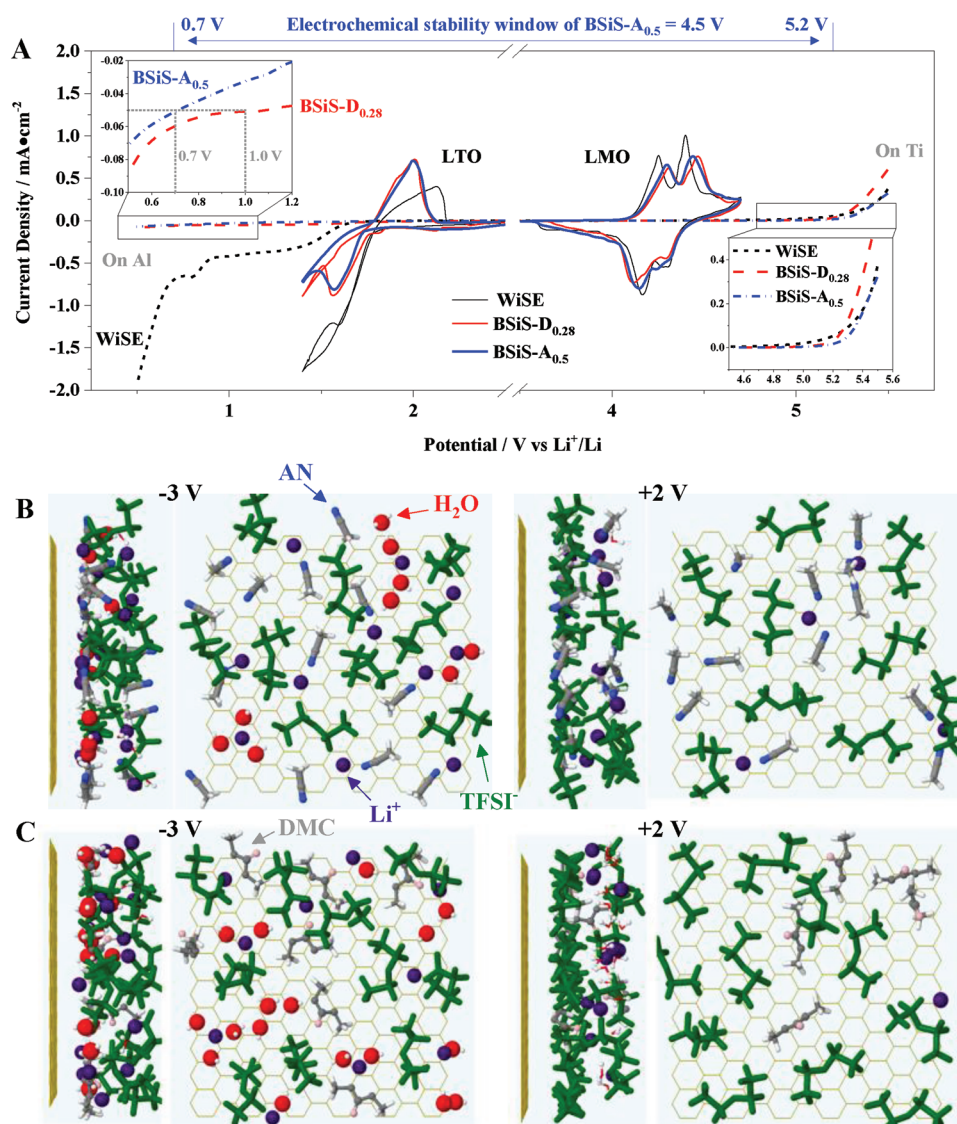


Figure 2. A) Electrochemical stability windows of WiSE, BSiS-D_{0.28}, and BSiS-A_{0.5} electrolytes measured with LSV (dashed lines) at the scan rate of 5 mV s⁻¹. The cathodic (from 3 to 0.5 V vs Li⁺/Li) and anodic (from 3 to 5.5 V vs Li⁺/Li) limits are tested by using Al and Ti as working electrodes, respectively. The heavy curves represent the CV of Li₄Ti₅O₁₂ (LTO) and LiMn₂O₄ (LMO) in WiSE, BSiS-D_{0.28}, and BSiS-A_{0.5} electrolytes at the scan rate of 0.1 mV s⁻¹. All measurements above are conducted in three-electrode devices with activated carbon and Ag/AgCl as counter and reference electrode, respectively. For convenience, the potential versus Ag/AgCl is converted to Li⁺/Li reference. Snapshots (including front and right side views) of inner-Helmholtz layer of negatively (left panel) and positively (right panel) charged electrodes obtained from MD simulation in B) BSiS-A_{0.5} and C) BSiS-D_{0.28} hybrid electrolytes.

Li⁺/Li in BSiS-D_{0.28} (Figure S10, Supporting Information) corresponds to the reduction of DMC-2Li⁺, while the onset of the second reduction occurred at 1.0 V versus Li⁺/Li corresponds to a major decomposition process that defines the cathodic limit. A reduction current density limit of around 0.05 mA cm⁻² was arbitrarily selected as the cut-off standard. It can be found from Figure S10 (Supporting Information) that the reduction current density of BSiS-A_{0.5} electrolyte reaches 0.05 mA cm⁻² at around 0.7 V versus Li⁺/Li. Therefore, it can be concluded that the presence of DMC and AN effectively postpones the cathodic limit down to 1.0 and 0.7 V versus Li⁺/Li, respectively. In addition, Videos S4 and S5 (Supporting Information) show that no visible hydrogen evolution occurs on Al with

the potential maintained at 1.0 V versus Li⁺/Li in BSiS-D_{0.28} and at 0.7 V versus Li⁺/Li in BSiS-A_{0.5}, while serious hydrogen evolutions occur in WiSE under the maintained potential of 1.0 V versus Li⁺/Li (Video S6, Supporting Information), confirming that BSiS-D_{0.28} and BSiS-A_{0.5} are stable on their own cathodic limit. According to the prediction of DFT calculation shown in Figure S3 (Supporting Information), the reduction activity of AN-2Li⁺ that exists in BSiS-A_{0.5} (see Figure 1A and Figure S7B, Supporting Information) is higher than DMC-2Li⁺, which could enable the formation of an interphase at a higher potential in the former. Even at potentials below 0.7 V versus Li⁺/Li, where the SEI formed by anions in WiSE fails to prevent hydrogen evolution, the detected reduction current of BSiS-A_{0.5}

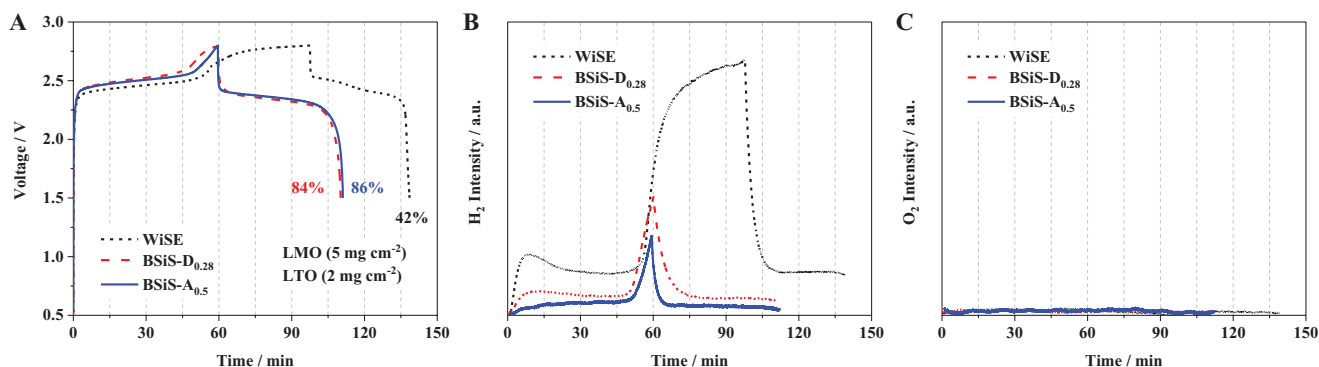


Figure 3. A) Initial charge/discharge curves of LMO/LTO cells (mass ratio 2.5:1) conducted in WiSE, BSiS-D_{0.28}, and BSiS-A_{0.5} electrolytes at 1 C (the rate is based on the mass of LTO), and corresponding B) H₂ and C) O₂ evolutions monitored via OLEMS under a continuous Ar flow.

electrolyte is smaller than that of BSiS-D_{0.28} electrolyte, indicating that the SEI originated from the AN-containing hybrid electrolyte functions as an effective kinetic barrier. According to the snapshots obtained from MD simulation of the interfacial electrolyte composition on negatively (left panel) and positively (right panel) charged electrodes, obviously much lower H₂O content is found at the negatively charged electrode surface in BSiS-A_{0.5} than that of BSiS-D_{0.28} (Figure 2B,C), therefore the introduction of AN assists excluding water molecules from the negatively charged electrode, which reduces the probability of water decomposition. Meanwhile, the inner Helmholtz layer formed in the BSiS-A_{0.5} electrolyte at the negative electrode not only has less water but also has more organic solvent compared to the BSiS-D_{0.28} electrolyte, which is partially due to higher molar fraction of AN versus DMC in the mixed water–organic solvent. Less adsorbed water for BSiS-A_{0.5} versus BSiS-D_{0.28} combined with the higher fraction of organic solvates (Li⁺-AN > Li⁺-DMC) leads to a more expedient and robust SEI formation for the AN-containing electrolytes (see Figure 2B,C). On the positively charged surface, H₂O molecules are excluded from the electrode surface together with Li⁺ due to the Coulombic repulsion. The interfacial layer is largely populated with anodic stable TFSI⁻ anions and AN solvent prevails, leading to high anodic stability of the hybrid electrolyte (Figure 2A). The higher oxidation current of BSiS-D_{0.28} in comparison with BSiS-A_{0.5} at high potentials is ascribed to the lower anodic stability of the linear carbonate DMC (Figure 2A,C, right panel).^[25–29] Overall, a 4.5 V electrochemical stability window is achieved due to the introduction of AN into aqueous electrolyte.

To further confirm the electrochemical stability obtained on inactive electrode, LTO and LMO were used as working electrodes, with their corresponding cyclic voltammograms (CVs) shown in Figure 2A. Because of the catalytic effect of titanate on water-splitting and relatively low lithium intercalation potential (1.55 V vs Li⁺/Li),^[11] WiSE itself fails to support its reversible operation (Figure 2A), while a reversible typical redox response of LTO can be easily observed in BSiS-A_{0.5} at very low rate of 0.1 mV s⁻¹ between 1.4 and 3 V versus Li⁺/Li. Although LTO can reversibly operate in BSiS-D_{0.28}, the lower cathodic current in BSiS-A_{0.5} at 1.4 V versus Li⁺/Li confirms its better cathodic stability. Lithiation–delithiation reaction of LMO electrode (Figure 2A) indicates that all electrolytes can support the reversible operation of LMO electrode without

water oxidation, however the reversibility decreases in the order of WiSE > BSiS-A_{0.5} > BSiS-D_{0.28}, which should be ascribed to the decrease of ionic conductivity (Figure 1D) and wettability of electrolytes with LMO electrodes (Figure S11, Supporting Information).

On-line electrochemical mass spectrometry (OLEMS) measurements were performed by using LMO/LTO cells (mass ratio 2.5:1) to analyze the formation of interphases during charge/discharge (Figure 3). Serious hydrogen evolution occurs during the initial charge/discharge process of the LMO/LTO cell with WiSE, along with a low Coulombic efficiency of 42%, which is in good agreement with the observed irreversible reduction of WiSE on LTO. Introducing AN and DMC co-solvents effectively suppresses the hydrogen evolution, with the former being more effective than the latter, confirming the higher interfacial stability brought by the AN co-solvent. Meanwhile, no visible oxygen evolution can be observed from LMO/LTO cells even during the initial charge/discharge. The highest Coulombic efficiency of LMO/LTO cell as obtained from BSiS-A_{0.5} (Figure 3A) should be therefore attributed to the improvements in the cathodic stability, which is further confirmed by the lower reduction residual current of chronoamperometric response with BSiS-A_{0.5} (Figure S12, Supporting Information). Moreover, such enhanced stability of LTO with AN-containing aqueous electrolyte significantly suppresses the parasitic degradation of LTO/LMO cells at 100% state-of-charge (SOC) (Figure S13, Supporting Information), where both discharge capacity and Coulombic efficiency are much superior in BSiS-A_{0.5} as compared with BSiS-D_{0.28}.

Since WiSE fails to stabilize LTO, the cycling stability of LMO/LTO cell in it suffers a high degradation at 1 C rate, as indicated by the initial and average Coulombic efficiency of 41% and 70.1% respectively, as well as the capacity retention of 6% after only 100 cycles (Figure 4A). Dramatically improved cycling stability is achieved with the introduction of DMC and especially AN. While 15% capacity retention after 300 cycles at an average Coulombic efficiency of 98.4% is obtained in BSiS-D_{0.28}, BSiS-A_{0.5} enables 98% capacity retention after 300 cycles in an average Coulombic efficiency of 98.7% along with initial capacity of 161 mAh g⁻¹ and initial Coulombic efficiency of 87%. The cycling performance in BSiS-A_{0.5} hybrid electrolyte is comparable with that in NCE at both ambient and sub-ambient temperatures with slightly higher capacity retention

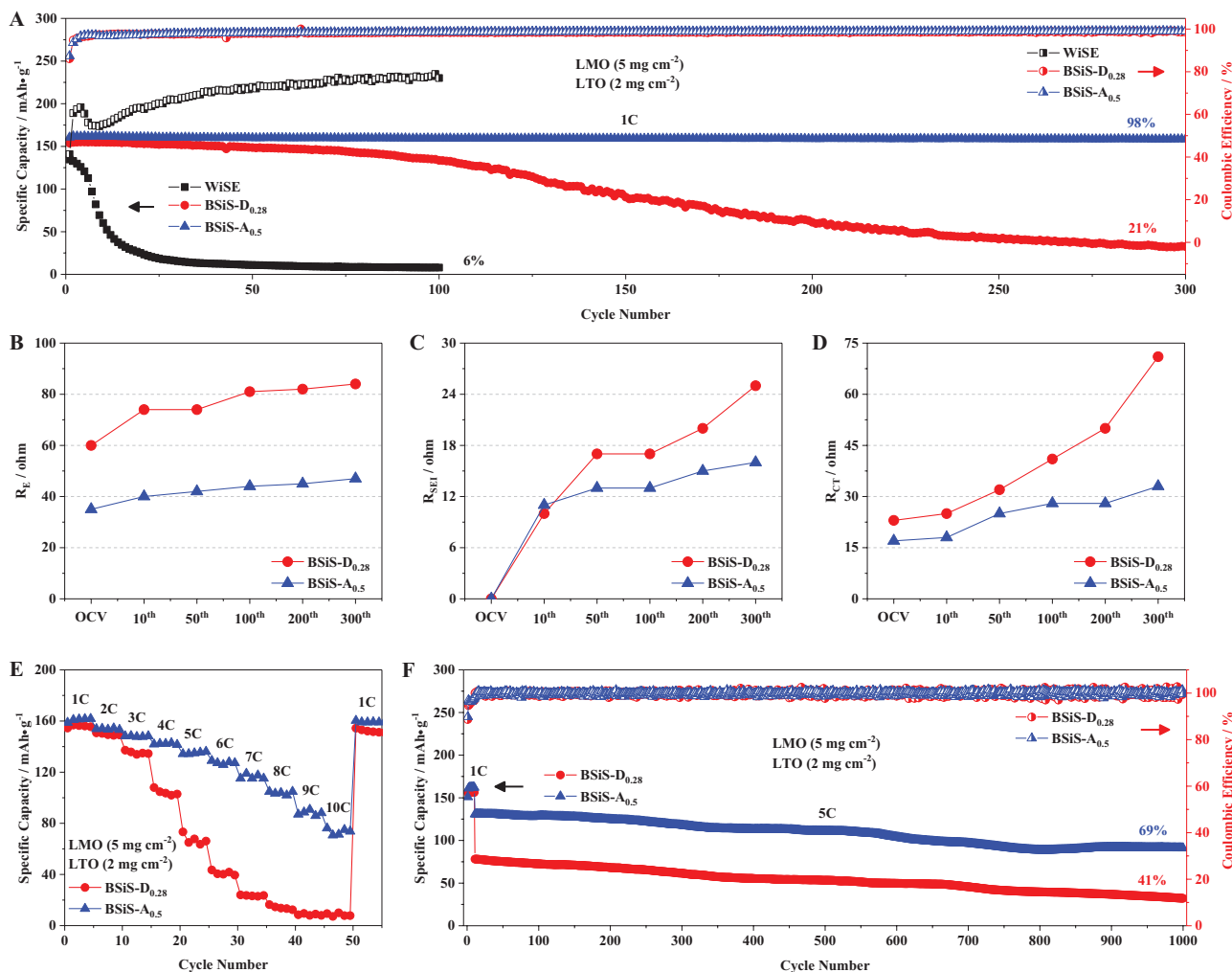


Figure 4. A) Cycling stability and Coulombic efficiency of LMO/LTO cells (mass ratio 2.5:1) operated in WiSE, BSiS-D_{0.28}, and BSiS-A_{0.5} electrolytes at 1 C, and corresponding B–D) fitting results of R_E , R_{SEI} , and R_{CT} obtained from EIS. F) Rate capability, and G) 5 C cycling stability including Coulombic efficiency of LMO/LTO cells (mass ratio 2.5:1) operated in BSiS-D_{0.28} and BSiS-A_{0.5} hybrid electrolytes. (Both capacity and rate are based on the mass of LTO.)

(Figure S14, Supporting Information), indicating that, beside the merits in safety and ambient-stability, such hybrid electrolyte does not compromise the electrochemical performance of the batteries. However, such excellent performance of BSiS-A_{0.5} electrolyte cannot be achieved when the LiTFSI salt concentration is decreased from 15.3 to 10 mol (Figure S15, Supporting Information), suggesting that a sufficiently high population of Li⁺ is needed to coordinate with H₂O and AN.

The electrochemical impedance spectra (EIS) were performed on LMO/LTO cells during cycling (Figure 4B–D and Figure S16, Supporting Information), which reveal that BSiS-A_{0.5} generates far lower cell impedances than BSiS-D_{0.28}, because of the higher ionic conductivity, lower interfacial resistance as well as better wettability of the former. The difference between these two electrolytes widens with the cycling, revealing that AN-based hybrid electrolyte produces a far more reliable interphase. With the lower resistance, LMO/LTO cell with BSiS-A_{0.5} hybrid electrolyte accordingly displays significantly greater rate

capability (Figure 4E,F). Even at 10 C rate, the LMO/LTO cell with BSiS-A_{0.5} maintains a discharge capacity of 76 mA h g⁻¹, in comparison with that of 9 mA h g⁻¹ with BSiS-D_{0.28}. Since low rate is the real test for electrolyte stability rather than number of cycles, we also subject the LMO/LTO cell containing BSiS-A_{0.5} to 0.2 C cycling (Figure S17, Supporting Information), where a high average Coulombic efficiency (> 96%) is displayed, further confirming the stability of BSiS-A_{0.5} hybrid electrolyte.

The chemical composition of interphases on LTO electrodes was investigated by X-ray photoelectron spectroscopy (XPS) after recovering LTO from a cell that experienced 300 cycles in BSiS-A_{0.5} at 1 C (Figure 5). C≡N species can be observed in both C 1s (287.0 eV)^[30] and N 1s (400.7 eV)^[25] spectra, which confirms that AN indeed participates in the interphasial chemistry. The other five C 1s peaks shown in Figure 5A include C–C species (284.8 eV)^[26] attributed to conductive agent acetylene black, C–H (285.6 eV)^[29] and CF₂ (291.1 eV)^[31] species arose from binder PVDF, C=O species (≈289.5 eV) corresponding to

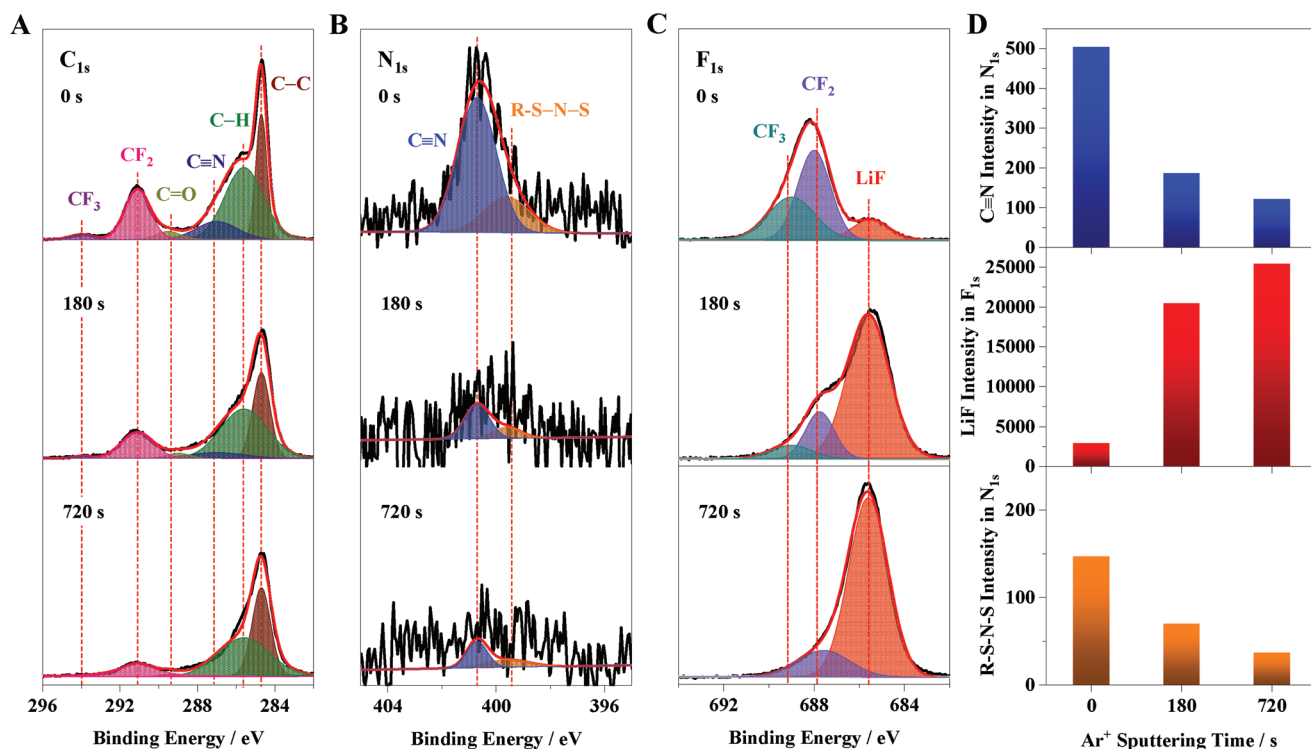


Figure 5. A) C 1s, B) N 1s, and C) F 1s XPS patterns of LTO with various durations of Ar⁺ sputtering after the cycling test of Figure 4A in BSiS-A_{0.5} hybrid electrolyte. D) The intensity changes of C≡N from N 1s, LiF from F 1s, and R-S-N-S from N 1s with various sputtering durations.

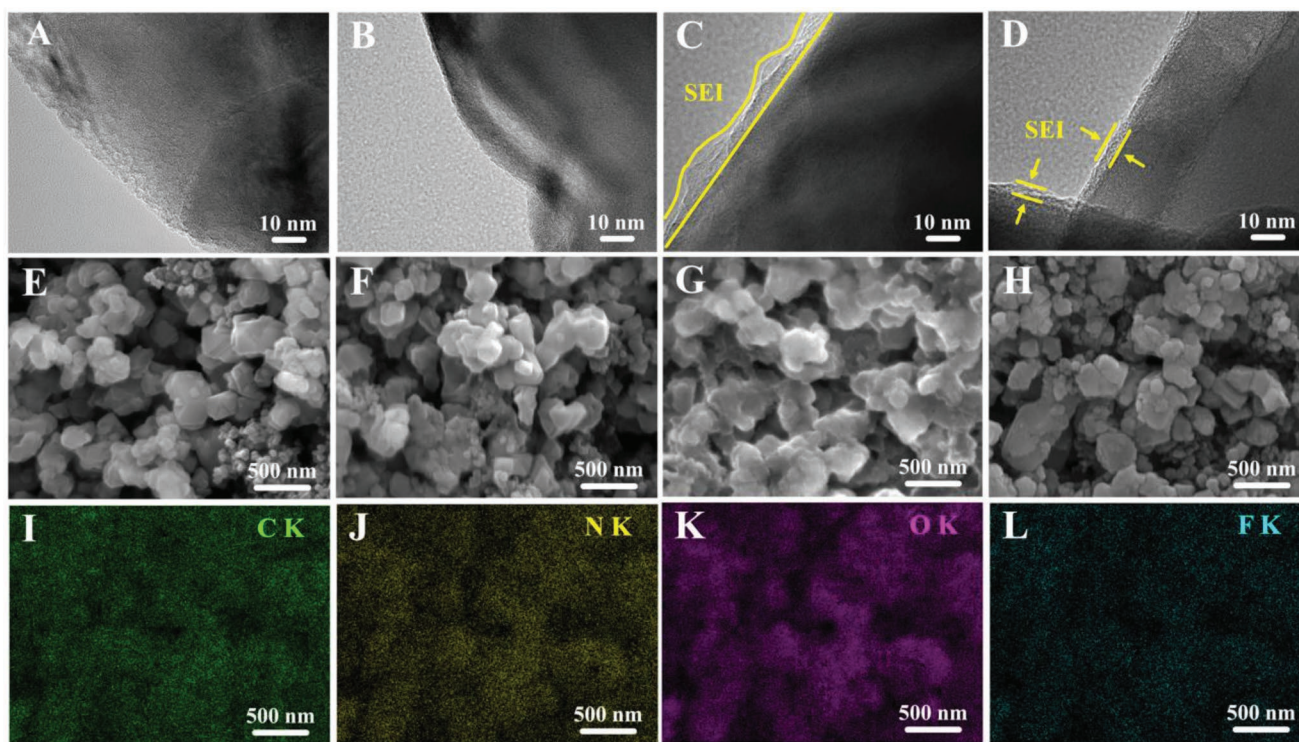


Figure 6. TEM and SEM images of A,E) fresh LTO and those after cycling test of Figure 4A in B,F) WiSE, C,G) BSiS-D_{0.28}, and D,H) BSiS-A_{0.5} electrolytes, together with I-L) elemental mapping images of cycled LTO in BSiS-A_{0.5} hybrid electrolyte.

Li_2CO_3 that should have resulted from the reduction of CO_2 dissolved in the electrolyte^[20] and CF_3 species (294.0 eV) coming from TFSI^- .^[9,10] Meanwhile, the reduction and film-forming reaction of TFSI^- can be also identified from the organic R-S-N-S species (399.6 eV) in N 1s and LiF (686.5 eV) in F 1s spectra.^[10,26] The depth profile of C 1s, N 1s, and F 1s spectra generated by Ar^+ sputtering reveal that the content of C≡N species from AN reduction decreases with the depth (Figure 5D top panels), while LiF displays the opposite trend (Figure 5D middle panels), suggesting a layered structure of SEI consisting of an inorganic inner and an AN-based outer layer, respectively, in good agreement with the higher reduction activity of TFSI^- than that of AN (Figure S3, Supporting Information). On the contrary, the outer content of R-N-S-N species, also generated

by TFSI^- reduction, is more abundant than inner layer (Figure 5D bottom panels). Transmission electron microscopy (TEM), scanning electron microscopy (SEM), and elemental mapping images of LTO, collected both before and after cycling, were given in Figure 6. No obvious deposition products can be observed on the LTO cycled in WiSE (Figure 6B,F), while LTO electrodes cycled in both BSiS- $\text{D}_{0.28}$ (Figure 6C,G) and BSiS- $\text{A}_{0.5}$ (Figure 6D,H) were covered by visible SEIs. In particular, the SEI observed on LTO recovered from BSiS- $\text{A}_{0.5}$ appears to be thinner and more uniform. The distribution of C, N, O and F elements on LTO from BSiS- $\text{A}_{0.5}$ (Figure 6I–L) further confirms the chemical homogeneity of its SEI. The surface of LMO before and after being cycled in BSiS- $\text{A}_{0.5}$ hybrid electrolyte was also examined under SEM and TEM (Figure S18, Supporting

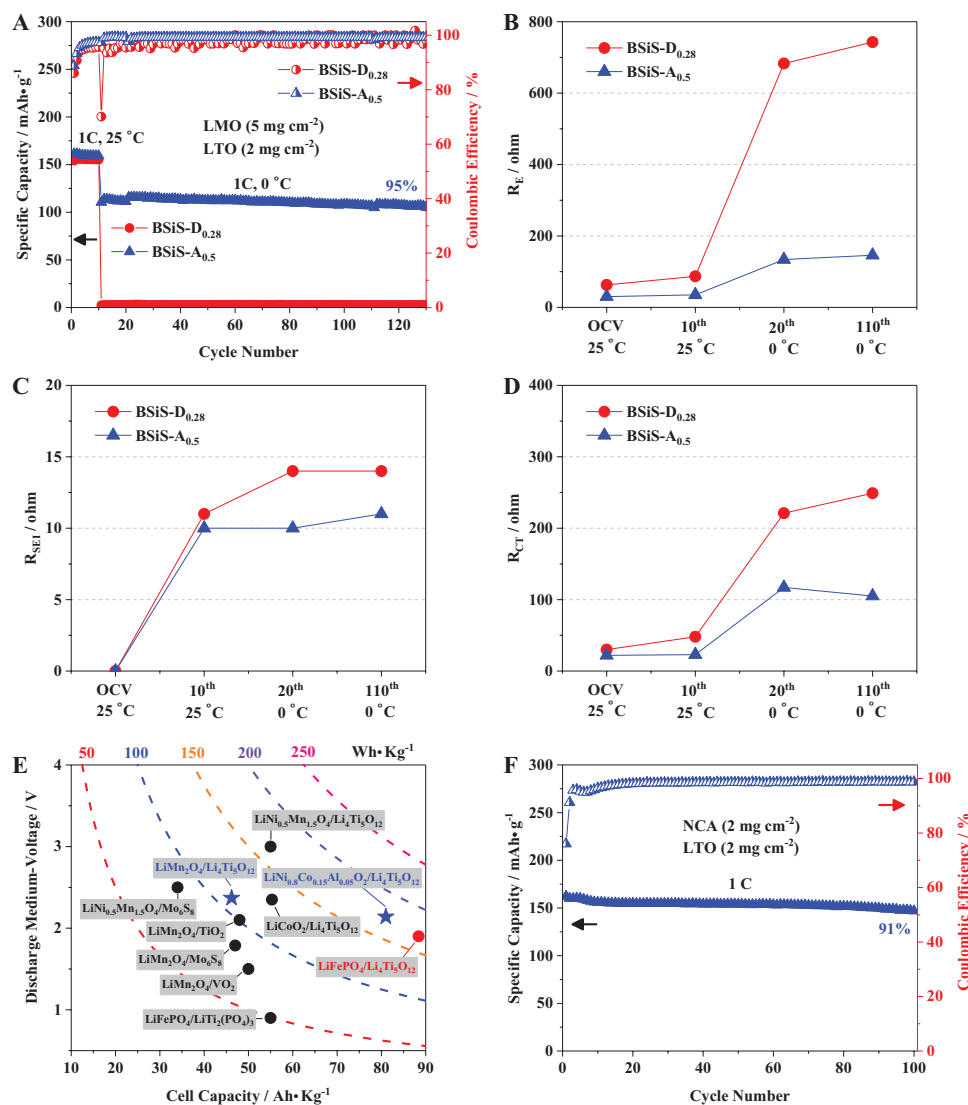


Figure 7. A) Cycling stability and Coulombic efficiency of LMO/LTO cells (mass ratio 2.5:1) operated in BSiS- $\text{D}_{0.28}$ and BSiS- $\text{A}_{0.5}$ hybrid electrolytes at 1 C under 0 °C after 10 cycles under 25 °C, and corresponding B–D) fitting results of R_E , R_{SEI} , and R_{CT} from EIS; E) Energy density of our LMO/LTO (mass ratio 2.5:1) and NCA/LTO (mass ratio 1:1) cells performed in BSiS- $\text{A}_{0.5}$ hybrid electrolyte (blue stars), compared with those performed in other aqueous and hybrid electrolytes (black circles) and nonaqueous electrolytes (red circles). The results are obtained from the first discharge curves and the cell capacity is based on total mass of cathode and anode active materials. F) Cycling stability and Coulombic efficiency of NCA/LTO cell (mass ratio 1:1) operated in BSiS- $\text{A}_{0.5}$ hybrid electrolyte at 1 C under 25 °C. (Both capacity and rate are based on the mass of LTO.)

Information), where a negligible difference can be detected, indicating the absence of electrolyte oxidation.

2.3. Widening Service Temperature Range and Supporting High Energy Density ALIBs

When charging and discharging LMO/LTO cells at 0 °C, the performance of the cell using BSiS-D_{0.28} experiences a steep drop to almost 0 mAh g⁻¹ (Figure 7A), which should be mainly ascribed to the sudden increase of R_E (Figure 7B and Figure S19, Supporting Information) induced by the deterioration in ionic conductivity (Figure 1E) and the solidification of electrolyte (Figure 1F).^[32] The cell using BSiS-A_{0.5}, in sharp contrast, retains a discharge capacity of 110 mAh g⁻¹ after 120 cycles at 0 °C, which accounts for 95% of the original capacity. The corresponding R_E in BSiS-A_{0.5} at 0 °C during cycling is obviously lower than BSiS-D_{0.28}, as evidenced by the changes of R_{S_{SEI}} and R_{CT} in both electrolytes (Figure 7C,D), in close similarity with those measured at room temperature (Figure 4C,D).

In addition to the extended service temperature range, BSiS-A_{0.5} also enables an ALIB constructed on higher energy density cathode LiNi_{0.8}Co_{0.15}Al_{0.05}O₂ (NCA). The initial energy density of NCA/LTO cell in BSiS-A_{0.5} hybrid electrolyte achieves 173 Wh kg⁻¹ (Figure S20, Supporting Information), which is higher than the data reported in literature (Figure 7E),^[3,6,9–12,33] some of which are even delivered in nonaqueous electrolytes (168 Wh kg⁻¹ for LiFePO₄/Li₄Ti₅O₁₂).^[34] Moreover, BSiS-A_{0.5} also supports such NCA/LTO cell with excellent cycling stability, with 91% retention of its initial discharge capacity (162 mAh g⁻¹) after 100 cycles at 1 C (Figure 7F).

3. Conclusion

A hybrid aqueous/nonaqueous electrolyte was designed in this work, which leverages merits of both co-solvents. The presence of AN decreases the interfacial water population at the negatively charged electrode surface, assists in generating an SEI consisting of both C≡N and R-S-N-S species in an organic outer and a LiF-rich inorganic inner layer. This hybrid SEI significantly suppresses the reduction of water, and extends electrochemical stability to the unprecedented range of 4.5 V. Moreover, the hybrid BSiS-A_{0.5} inherits the nonflammable nature of aqueous electrolyte, and enables LTO anode to couple with both LMO and higher energy density NCA with excellent cycling stability, rate capability, and low-temperature performance. This new class of aqueous/nonaqueous hybrid electrolytes should find extensive applications where both high energy and safety are required.

Supporting Information

Supporting Information is available from the Wiley Online Library or from the author.

Acknowledgements

This work was supported by the National Natural Science Foundation of China (21573080), the Guangdong Program for Support of Top-notch

Young Professionals (2015TQ01N870) and Distinguished Young Scholar (2017B030306013), and the Science and Technology Planning Project of Guangdong Province (2017B090901020).

Conflict of Interest

The authors declare no conflict of interest.

Keywords

acetonitrile, aqueous lithium-ion batteries, aqueous/nonaqueous hybrid electrolytes, electrochemical stabilities, low-temperature performance

Received: August 14, 2019

Revised: November 7, 2019

Published online: November 22, 2019

- [1] M. Armand, J.-M. Tarascon, *Nature* **2008**, *451*, 652.
- [2] M. Winter, B. Barnett, K. Xu, *Chem. Rev.* **2018**, *118*, 11433.
- [3] J. Y. Luo, W. J. Cui, P. He, Y. Y. Xia, *Nat. Chem.* **2010**, *2*, 760.
- [4] C. Yang, J. Chen, T. Qing, X. Fan, W. Sun, A. von Wald Cresce, M. S. Ding, O. Borodin, J. Vatamanu, M. A. Schroeder, N. Eidson, C. Wang, K. Xu, *Joule* **2017**, *1*, 122.
- [5] J. F. Parker, C. N. Chervin, I. R. Pala, M. Machler, M. F. Burz, J. W. Long, D. R. Rolison, *Science* **2017**, *356*, 415.
- [6] W. Li, J. R. Dahn, D. S. Wainwright, *Science* **1994**, *264*, 1115.
- [7] Y. Wang, J. Yi, Y. Xia, *Adv. Energy Mater.* **2012**, *2*, 830.
- [8] K. Xu, C. Wang, *Nat. Energy* **2016**, *1*, 16161.
- [9] L. Suo, O. Borodin, T. Gao, M. Olguin, J. Ho, X. Fan, C. Luo, C. Wang, K. Xu, *Science* **2015**, *350*, 938.
- [10] Y. Yamada, K. Usui, K. Sodeyama, S. Ko, Y. Tateyama, A. Yamada, *Nat. Energy* **2016**, *1*, 16129.
- [11] L. Suo, O. Borodin, W. Sun, X. Fan, C. Yang, F. Wang, T. Gao, Z. Ma, M. Schroeder, A. von Wald Cresce, S. M. Russell, M. Armand, A. Angell, K. Xu, C. Wang, *Angew. Chem., Int. Ed.* **2016**, *55*, 7136.
- [12] F. Wang, O. Borodin, M. S. Ding, M. Gobet, J. Vatamanu, X. Fan, T. Gao, N. Edison, Y. Liang, W. Sun, S. Greenbaum, K. Xu, C. Wang, *Joule* **2018**, *2*, 927.
- [13] C. H. Yim, J. Tam, H. Soboleski, Y. Abu-Lebdeh, *J. Electrochem. Soc.* **2017**, *164*, A1002.
- [14] K. Xu, *Chem. Rev.* **2004**, *104*, 4303.
- [15] Q. Dou, S. Lei, D. Wang, Q. Zhang, D. Xiao, H. Guo, A. Wang, H. Yang, Y. Li, S. Shi, X. Yan, *Energy Environ. Sci.* **2018**, *11*, 3212.
- [16] O. Borodin, L. Suo, M. Gobet, X. Ren, F. Wang, A. Faraone, J. Peng, M. Olguin, M. Schroeder, M. S. Ding, E. Gobrogge, A. von Wald Cresce, S. Munoz, J. A. Dura, S. Greenbaum, C. Wang, K. Xu, *ACS Nano* **2017**, *11*, 10462.
- [17] N. D. Trinh, D. Lepage, D. Aymé-Perrot, A. Badia, M. Dollé, D. Rochefort, *Angew. Chem., Int. Ed.* **2018**, *57*, 5072.
- [18] Y. Yamada, K. Furukawa, K. Sodeyama, K. Kikuchi, M. Yaegashi, Y. Tateyama, A. Yamada, *J. Am. Chem. Soc.* **2014**, *136*, 5039.
- [19] J. Zheng, G. Tan, P. Shan, T. Liu, J. Hu, Y. Feng, L. Yang, M. Zhang, Z. Chen, Y. Lin, J. Lu, J. C. Neuefeind, Y. Ren, K. Amine, L. W. Wang, K. Xu, F. Pan, *Chem* **2018**, *4*, 2872.
- [20] L. Suo, D. Oh, Y. Lin, Z. Zhuo, O. Borodin, T. Gao, F. Wang, A. Kushima, Z. Wang, H. C. Kim, Y. Qi, W. Yang, F. Pan, J. Li, K. Xu, C. Wang, *J. Am. Chem. Soc.* **2017**, *139*, 18670.
- [21] X. Ren, S. Chen, H. Lee, D. Mei, M. H. Engelhard, S. D. Burton, W. Zhao, J. Zheng, Q. Li, M. S. Ding, M. Schroeder, J. Alvarado, K. Xu, Y. S. Meng, J. Liu, J. G. Zhang, W. Xu, *Chem* **2018**, *4*, 1877.

- [22] S. Chen, J. Zheng, L. Yu, X. Ren, M. H. Engelhard, C. Niu, H. Lee, W. Xu, J. Xiao, J. Liu, J. G. Zhang, *Joule* **2018**, 2, 1548.
- [23] J. Wang, Y. Yamada, K. Sodeyama, E. Watanabe, K. Takada, Y. Tateyama, A. Yamada, *Nat. Energy* **2018**, 3, 22.
- [24] H. Duncan, N. Salem, Y. Abu-Lebdeh, *J. Electrochem. Soc.* **2013**, 160, A838.
- [25] H. Zhi, L. Xing, X. Zheng, K. Xu, W. Li, *J. Phys. Chem. Lett.* **2017**, 8, 6048.
- [26] J. Chen, L. Xing, X. Yang, X. Liu, T. Li, W. Li, *Electrochim. Acta* **2018**, 290, 568.
- [27] X. Yang, J. Chen, Q. Zheng, W. Tu, L. Xing, Y. Liao, M. Xu, Q. Huang, G. Cao, W. Li, *J. Mater. Chem. A* **2018**, 6, 16149.
- [28] B. Liao, H. Li, M. Xu, L. Xing, Y. Liao, X. Ren, W. Fan, L. Yu, K. Xu, W. Li, *Adv. Energy Mater.* **2018**, 8, 1800802.
- [29] Y. Zhu, X. Luo, H. Zhi, Y. Liao, L. Xing, M. Xu, X. Liu, K. Xu, W. Li, *J. Mater. Chem. A* **2018**, 6, 10990.
- [30] G. Deniau, G. Lécayon, P. Viel, G. Hennico, J. Delhalle, *Langmuir* **1992**, 8, 267.
- [31] X. Zheng, X. Wang, X. Cai, L. Xing, M. Xu, Y. Liao, X. Li, W. Li, *ACS Appl. Mater. Interfaces* **2016**, 8, 30116.
- [32] M. Ding, K. Xu, T. Jow, *J. Therm. Anal. Calorim.* **2000**, 62, 177.
- [33] F. Wang, L. Suo, Y. Liang, C. Yang, F. Han, T. Gao, W. Sun, C. Wang, *Adv. Energy Mater.* **2017**, 7, 1600922.
- [34] C. M. Julien, K. Zaghib, A. Mauger, H. Groult, *Adv. Chem. Eng. Sci.* **2012**, 02, 321.